Far-infrared absorption of undoped and Br-doped carbon nanofiber powder in stacked-cup cone configuration

Naween Anand [1,2,*], Charles Bruce,[3,†] A. F. Hebard [1,‡] and D. B. Tanner [1,§]

[1]*Department of Physics, University of Florida, Gainesville, Florida 32611-8440, USA*
[2]*Materials Science Division, Argonne National Laboratory, Argonne, Illinois 60439, USA*
[3]*Department of Physics, MSC 3D, New Mexico State University, Las Cruces, New Mexico 88003-8001, USA*

We performed room-temperature far-infrared (40–650 cm^{-1}) transmission measurements on undoped and bromine-doped powder samples of carbon nanofibers in stacked-cup cone geometry. The transmission spectra show enhanced transmittance after bromine doping and all spectra were fit to a Drude-Lorentz (DL) model. A decreased metallic conductivity along with a redshift of the lowest semiconducting gap was found with doped samples. A significant decrease in the scattering rate upon heavy doping has been qualitatively explained as partial ordering of intercalated dopant ions. Absorption spectra were derived from the transmission spectra under the assumption of nondispersive reflectance and subsequently compared with DL-model-derived spectra. The free-carrier density of the *n*-type powder and the electronic mean free path were estimated and compared with reported values for single-walled nanotubes and pyrolytic graphite.

I. INTRODUCTION

The unique electronic and mechanical properties of carbon nanotubes (CNTs) have caused much interest among researchers since their discovery [1]. CNTs constitute a new class of materials that could contribute to the development of novel nanoscale electronic devices [2–8]. Isolated single-walled nanotubes (SWNTs) and bundled nanoropes have been studied extensively and are reported to have either metallic or semiconducting phases, based on their (*n, m*) wrapping vector indices [9–12]. The related materials, carbon nanofibers (CNFs), also known as stacked-cup carbon nanotubes (SCC-NTs), are bigger in diameter than carbon nanotubes. They are highly graphitic carbon nanomaterials with excellent mechanical properties, and electrical and thermal conductivity, all strongly dependent on growth technique and high-temperature heat treatment routine [13–18]. These properties make them suitable for various applications such as radio-frequency interference shields, electrostatic painting, electrostatic discharge probes, and reinforcing composites for industrial applications [19].

Structural characteristics such as diameter, length, chirality, and defects, which essentially dictate all important properties in SCCNTs and related carbon forms, are difficult to control during synthesis. Therefore, a great deal of interest towards controlling their properties through extrinsic doping methods has been observed lately [20–23]. The study of doping behavior gets somewhat convoluted because of the mixed metallic and semiconducting phases coexisting in most carbon nanomaterials. Nonetheless, the doping process alters the valence- and conduction-band statistics and also the free-carrier dynamics in these systems, just like it does in graphite. Hence, it serves as a tool for the tuning of electronic and mechanical properties [24,25]. A previous study of bromine intercalation in highly oriented pyrolytic graphite (HOPG) has demonstrated a pathway to weaken the interplanar coupling between individual layers, pushing the system towards an ordered stack of graphene sheets, possibly dominated by Dirac fermions. Bromine doping has resulted in enhanced carrier density per carbon, higher mobility along the graphite plane, and reduced conductance along the interplanar direction, attributed to weakened interplanar coupling [26]. Such direct tuning of electronic properties in carbon nanomaterials is highly desirable for its potential electronic applications. Frequency-dependent optical studies of doped and undoped carbon nanomaterials have shown that there is low-frequency metallic behavior coexisting with a small-band-gap (around 8 meV) semiconducting phase. Moreover, higher-frequency-range studies have shown the electronic band structure tuning upon *p*-type (I$_2$, Br$_2$, N$_2$) and *n*-type (K, Cs, organic radical anions) doping [20,27–30]. This article is focused on investigating the absorption and conductive properties of carbon nanofibers in the stacked-cup cone configuration through optical measurements. It also explores the possibility of tuning these properties through an acceptorlike dopant at low and high concentrations.

II. EXPERIMENTAL PROCEDURE AND RESULTS

Transmission electron microscope (TEM) images shown in Fig. 1 give details about the structural features of the powder

*nanand@anl.gov
†cbruce@nmsu.edu
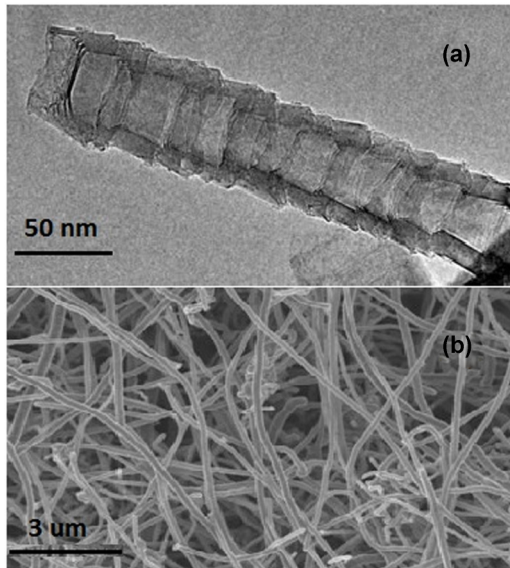‡afh@phys.ufl.edu
§tanner@phys.ufl.edu

FIG. 1. (a) High-resolution TEM image of single carbon nanofiber showing stacked-cup cone structure. (b) TEM image of Pyrograf III carbon nanofiber powder [31].

FIG. 2. Room-temperature transmittance spectra of Br-doped and undoped CNF powder for different thicknesses.

sample. High-quality samples (Pyrograf III, CNF PR-25-XT-PS) were prepared by Applied Sciences, Inc. These samples have a unique structure in which the graphene plane surface is canted from the fiber axis exposing the plane edges present on the interior and exterior surfaces of the carbon nanofibers. High-resolution TEM images shown in Fig. 1(a) verify the structural integrity of the sample where the canted stacking of folded graphene sheets is apparent. These folded sheets make nanofibers with diameter varying between 60 and 150 nm. The fibers were pyrolytically stripped, making them free from any chemical vapor deposition carbon and polyaromatic hydrocarbon contamination on the surface. The large-area TEM image in Fig. 1(b) suggests that these nanofibers vary in length from tenths to tens of micrometers [13].

Transmission spectra were acquired in the far-infrared range (40–650 cm^{-1}) at room temperature using a Bruker 113v Fourier-transform interferometer. A helium-cooled silicon bolometer detector was used in this spectral range. A homogeneous layer of CNF powder of thickness 0.25, 0.15, or 0.10 mm was uniformly spread between two polyethylene windows. The sample holder had a 6-mm aperture. Subsequently, to study the effect of bromine intercalation, the transmission measurements were repeated under identical conditions immediately after exposing powder samples to Br$_2$ for 10 min and 100 min, respectively. The extent of bromine doping was estimated by observing the change in the density of the sample powder. The density of the undoped sample was estimated to be around 0.3 g/cm^3. This density increases to 0.39 g/cm^3 after 10 min of bromine exposure, changing the stoichiometry to CBr$_{0.045}$. A bromine exposure time of 100 min resulted in a doped powder of CBr$_{0.14}$ stoichiometry with density around 0.58 g/cm^3. The polyethylene windows introduced interference fringes in the transmission spectra which were removed using a Fourier-transform smoothing technique. The fringe removal routine did not change the level of transmission.
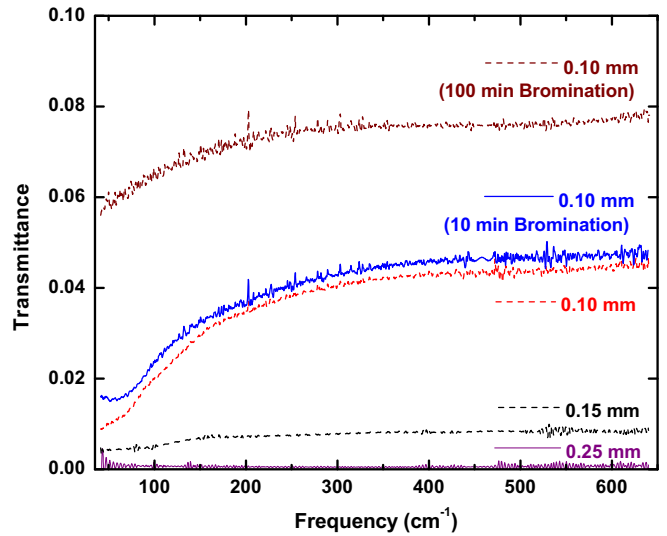
Figure 2 shows the room-temperature transmission spectra of the undoped CNF sample for different thicknesses as well as the spectra after bromination. We observed negligible transmission for the 0.25-mm sample thickness. The transmission level increases slightly as the thickness decreases to 0.15 mm but is still below 1% in the entire far-infrared range. However, we observed a notable increase in the transmission as thickness is decreased to 0.10 mm. The transmission decreases from about 5% to 1% as frequency decreases from 650 to 40 cm^{-1}. The transmission starts decreasing more quickly around 150 cm^{-1}; this behavior can also be seen in the spectra of the 0.15-mm-thick sample. All further measurements and analyses were conducted with the 0.10-mm-thick powder sample. The transmission measurements were repeated immediately after brominating two powder samples, one for 10 min and one for 100 min. The transmission of the powder sample brominated for 10 min is quite similar to the undoped sample, except for a more obvious onset of increased transmission at low frequencies. In contrast, the transmission of the sample brominated for 100 min is substantially increased over the entire frequency range.

III. ANALYSIS

A. Drude-Lorentz model fits

A Drude-Lorentz model was used to fit the transmission data of the CNF powder sample. Figure 3 shows the Drude-Lorentz fit to the transmission data. The Drude component characterizes the free carriers and their dynamics at zero frequency. On the other hand, the Lorentz contributions are included to account for the electronic transitions, due to the low gap semiconducting phase of the sample and the higher energy transitions. The dielectric function is [32,33]

$$\varepsilon(\omega) = \varepsilon_\infty - \frac{\omega_{p0}^2}{\omega^2 + i\omega/\tau} + \sum_{j=1}^{4} \frac{\omega_{pj}^2}{\omega_j^2 - \omega^2 - i\omega\gamma_j}, \quad (1)$$
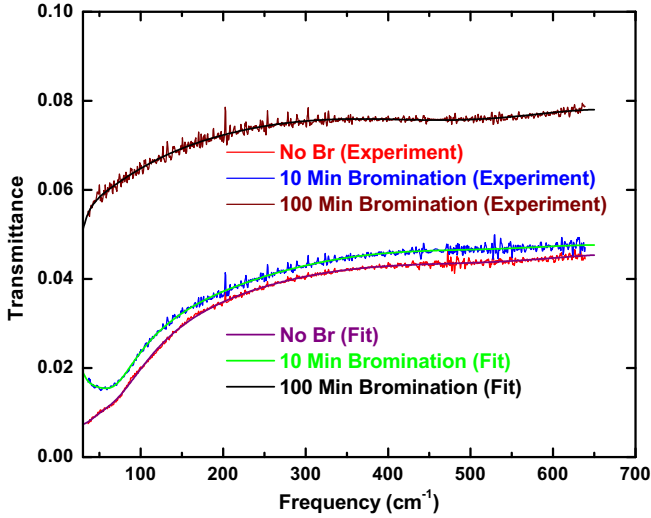
FIG. 3. Drude-Lorentz fit to the transmittance spectra of 0.10-mm-thick Br-doped and undoped CNF powder at room temperature.
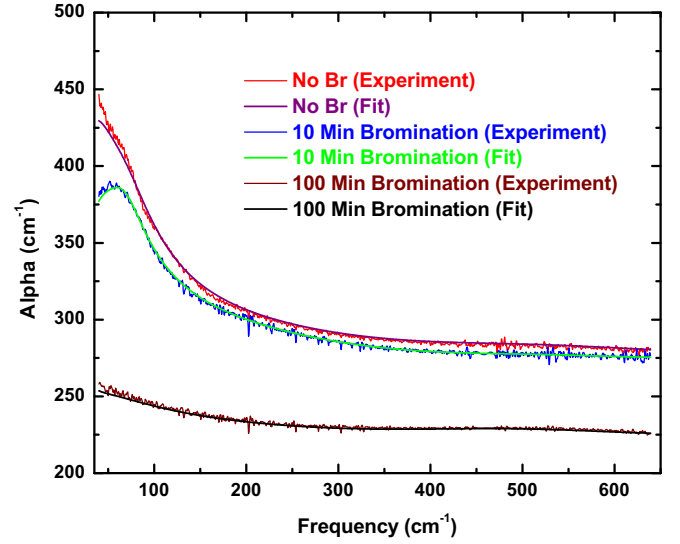

FIG. 4. A comparison between the transmission-based absorption coefficient and the Drude-Lorentz-parameter-computed absorption coefficient for the Br-doped and undoped samples.

where the first term represents the core electron contribution (transitions above the measured range), the second term is the free-carrier contribution, characterized by Drude plasma frequency ω_{p0} and free carrier relaxation time τ, and the third term is the sum of four Lorentzian oscillators representing electronic contributions to the dielectric function. The Lorentzian parameters are the jth oscillator plasma frequency ω_{pj}, its central frequency ω_j, and its linewidth γ_j. Our nonlinear least-squares fitting routine calculates the dielectric function using all the fitting parameters and in addition the thickness. The transmittance calculation assumed thick samples, averaging over interference patterns [33]. The best least-squares fit parameters give 13% for the single surface reflectance. This value is typical for carbon-based metamaterials in the far-infrared region [34].

Table I lists the parameters for the Drude term along with the four Lorentzian terms. There were no obvious vibrational

features observed in any of the samples. All three samples were identified as being in a mixed metallic phase of CNF bundles along with a low-gap semiconducting phase. In many previous studies, this semiconducting gap in CNTs around 8 meV has been attributed to either the curvature-induced gap or the symmetry breaking among neighboring tubes in metallic phase [12,35,36].

B. Far-infrared characteristics

Next, the absorption coefficient was computed from the transmission data by inverting [32,33]

$$\Im = \frac{(1 - \Re_{sb})^2 e^{-\alpha d}}{1 - \Re_{sb}^2 e^{-2\alpha d}} \tag{2}$$

where d is the thickness and $\Re_{sb}$ is the "single-bounce" reflectance (the reflectance of a single surface). This equation is quadratic in $e^{\alpha d}$ with one positive root,

$$e^{\alpha d} = \frac{(1 - \Re_{sb})^2}{\Im}\left[1/2 + \sqrt{1/4 + \frac{\Re_{sb}^2 \Im^2}{(1 - \Re_{sb})^4}}\right], \tag{3}$$

where $\Re_{sb} = 0.13$ was estimated using the DL parameters from Table I [32,33]. A comparison between the absorption coefficient α, derived from the transmission spectra using Eq. (3) and the calculated absorption coefficient using the set of DL parameters from Table I, is shown in Fig. 4. It shows a clear decrease in the absorption coefficient with Br doping in the entire measurement range. This strong agreement between the two spectra gives us confidence in the fitting procedure and the transmission-based absorption coefficient estimation routine.

We interpret the rise in absorption below 150 cm^{-1} as due to free carriers in the samples. This interpretation is confirmed by the conductivity spectrum calculated from the same set of DL parameters. The conductivity is shown in Fig. 5. The real part of the optical conductivity is $\sigma_1 = (\omega \varepsilon_2)/4\pi$,

TABLE I. Drude-Lorentz parameters for undoped and Br-doped samples at room temperature (300 K).

Mode assignment	Symbol	No Br (cm^{-1})	10 min (cm^{-1})	100 min (cm^{-1})
Drude component metallic phase	ω_{p0}	73	65	41
	$1/\tau$	33	41	15
Low-gap semiconducting phase	ω_{p1}	30	24	25
	ω_1	69	67	43
	γ_1	80	53	112
Electronic excitation 2	ω_{p2}	264	262	256
	ω_2	137	139	132
	γ_2	838	829	850
Electronic excitation 3	ω_{p3}	110	104	103
	ω_3	616	613	613
	γ_3	696	672	709
Electronic excitation 4	ω_{p4}	202	220	186
	ω_4	1098	1098	1082
	γ_4	562	528	561

FIG. 5. The Drude-Lorentz-parameter-computed optical conductivity for the Br-doped and undoped samples.

FIG. 6. The effect of bromination of CNF powder on (a) low gap excitation conductivity contribution and (b) Drude conductivity contribution at room temperature.

where ε_2 represents the imaginary part of the dielectric function in Eq. (1). There is a free-carrier absorption rise at the lowest measured frequency, which rolls off as the frequency reaches the Drude relaxation rate $1/\tau$. A small overlapping absorption shoulder around 50–80 cm^{-1} can also be observed, which is attributed to the low-gap semiconducting component in the CNF powder sample. The optical conductivity, especially the Drude contribution, decreases with increasing bromine intercalation. This change can also be quantitatively seen in Table I, where the Drude plasma frequency for the 100-min sample drops to almost half of that for the undoped sample even as the scattering time τ gets doubled.

Figure 6(a) shows the conductivity contribution from the lowest electronic transition due to the semiconducting phase, whereas the Drude conductivity from the metallic phase is shown in Fig. 6(b). The semiconducting gap (around 8 meV for the undoped sample) shifts towards lower frequencies after 100 minutes of bromination. The strength of this electronic transition also decreases and becomes much broader with bromination. As the DL parameters suggest, the Drude conductivity decreases with bromination and the scattering rate surprisingly drops down significantly for the 100-min sample. (A drop in scattering rate means an increase in mean free time for the charge carriers.)

IV. DISCUSSION AND CONCLUSIONS

The amphoteric behavior of carbon nanomaterials and changes in their transport properties upon doping have been qualitatively explained in terms of the charge-transfer mechanism in the framework of the rigid band model [20]. Doping with bromine modifies the structural framework of the nanofibers by occupying the endohedral sites or interstitial sites, or by substituting carbon from the tube surface and forming heteronanofibers as shown in previous studies [23,29,30]. In HOPG, it has been shown that transport properties are highly anisotropic and that the anisotropy gets even more pronounced upon doping. While a small charge transfer
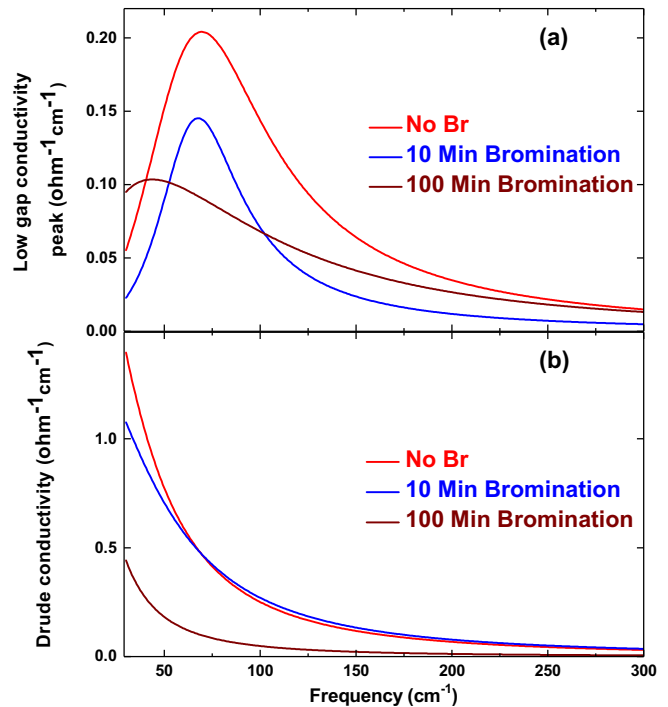
from intercalated bromine atoms enhances the carrier density per carbon and makes the transport along the sheet more metallic, it also suppresses the conductivity along the perpendicular direction by decreasing the tunneling probability between sheets by acting like a negative pressure, pushing them apart [26]. However, for a sample in powder form with randomly oriented fiber axes, one can only measure a conductivity which is an average over all orientations. In a nitrogen-doped CNF transport study, it was shown that a higher level of doping increases the number or severity of defects in the fiber, thereby decreasing the carrier mobility and conductivity [30]. On the contrary, our measurements indicated a slight increase of scattering rate in the 10-min sample, is followed by a 50% drop in $1/\tau$ for the 100-min sample, as compared to the undoped sample. This experimental observation is rather surprising; however, similar effects were seen in Br-intercalated graphite [26]. A fivefold decrease of $1/\tau$ with heavy Br doping in highly oriented graphite was qualitatively explained due to the partial ordering of Br ions. In addition, enhanced carrier mobilities have been observed in several modulation-doped semiconductor heterostructures due to partial ordering of donors [37–39]. Based on these studies, an argument could be made that the heavy bromination in stacked CNFs may develop minibands of dopant states due to the formation of a laminar structure of entirely uncorrelated ordered layers of bromine ions without any three-dimensional ordering. This partial ordering perhaps leads to a suppressed scattering rate of charge carriers, as observed in our measurements.

Heavy doping has also resulted in a decrease in the Drude plasma frequency and slight redshift of the semiconducting gap. A reduction in the semiconducting gap and the optical

conductivity after bromination suggests that the undoped CNF powder has an excess of n-type carriers. These carriers partially get neutralized by bromination. Assuming that $m^* \approx m_e$, the Drude plasma frequency ω_{p0} for the undoped sample implies a charge carrier density $n \approx 6 \times 10^{16}$ cm^{-3}. The density of the undoped powder is about $\rho \approx 0.3$ g/cm^3, compared to the ideal SWNT density of $\rho \approx 2$ g/cm^3. Adjusting for the low density of the CNF powder sample and further assuming that about half of the sample stays in the metallic CNF bundle phase [40–42], the adjusted free-carrier density of the metallic component of the sample is around $n \approx 1 \times 10^{18}$ cm^{-3}, an order of magnitude smaller than in pyrolytic graphite at room temperature [43]. Moreover, it was reported in previous studies that only a fraction of the charge carriers contribute to delocalized charge transport in CNT mat structure, while the remaining localized fraction of charge carriers make a smaller contribution to the Drude conductivity, leading to a reduced carrier density estimation [41,44]. The Drude scattering rate of the charge carriers in the undoped sample leads to a mean

free time $\tau \approx 1.6 \times 10^{-13}$ s, comparable to the result found in a previous study for CNTs in mat structure [41]. Using the Fermi velocity of graphite, $\upsilon_F \approx 8 \times 10^5$ m/s, we estimate the mean free path to be about $\Lambda \approx 120$ nm. The mean free path after 100 min of bromination is about twice this value. Some of the higher-energy electronic excitations show very large linewidths. This behavior is expected; the linewidths of these interband transitions are due to the details of the electronic structure in a possibly inhomogeneous system and not to the lifetime effects. These parameters show very weak dependence on doping.

[1] S. Iijima, Nature **354**, 56 (1991).

[2] T. W. Ebbesen, H. J. Lezec, H. Hiura, J. W. Bennett, H. F. Ghaemi, and T. Thio, Nature **382**, 54 (1996).

[3] S. J. Tans, M. H. Devoret, H. Dai, A. Thess, R. E. Smalley, L. J. Geerligs, and C. Dekker, Nature **386**, 474 (1997).

[4] S. Saito, Science **278**, 77 (1997).

[5] L. Chico, V. H. Crespi, L. X. Benedict, S. G. Louie, and M. L. Cohen, Phys. Rev. Lett. **76**, 971 (1996).

[6] M. Bockrath, D. H. Cobden, P. L. McEuen, N. G. Chopra, A. Zettl, A. Thess, and R. E. Smalley, Science **275**, 1922 (1997).

[7] E. W. Wong, P. E. Sheehan, and C. M. Lieber, Science **277**, 1971 (1997).

[8] M. Buongiorno Nardelli, B. I. Yakobson, and J. Bernholc, Phys. Rev. B **57**, R4277 (1998).

[9] M. S. Dresselhaus, G. Dresselhaus, and R. Saito, Phys. Rev. B **45**, 6234 (1992).

[10] J. W. Mintmire, B. I. Dunlap, and C. T. White, Phys. Rev. Lett. **68**, 631 (1992).

[11] N. Hamada, S.-i. Sawada, and A. Oshiyama, Phys. Rev. Lett. **68**, 1579 (1992).

[12] C. L. Kane and E. J. Mele, Phys. Rev. Lett. **78**, 1932 (1997).

[13] C. W. Bruce and S. Alyones, Appl. Opt. **51**, 3250 (2012).

[14] J. Howe, G. Tibbetts, C. Kwag, and M. Lake, J. Mater. Res. **21**, 2646 (2006).

[15] M. Endo, Y. Kim, T. Hayashi, T. Yanagisawa, H. Muramatsu, M. Ezaka, H. Terrones, M. Terrones, and M. Dresselhaus, Carbon **41**, 1941 (2003).

[16] G. G. Tibbetts, M. L. Lake, K. L. Strong, and B. P. Rice, Compos. Sci. Technol. **67**, 1709 (2007).

[17] D. Shimamoto, K. Fujisawa, H. Muramatsu, T. Hayashi, Y. A. Kim, T. Yanagisawa, M. Endo, and M. S. Dresselhaus, Carbon **48**, 3643 (2010).

[18] H. Darmstadt, C. Roy, S. Kaliaguine, J.-M. Ting, and R. L. Alig, Carbon **36**, 1183 (1998).

[19] K. Okuda, Tanso **1992**, 426 (1992).

[20] S. Kazaoui, N. Minami, R. Jacquemin, H. Kataura, and Y. Achiba, Phys. Rev. B **60**, 13339 (1999).

[21] B. Ruzicka, L. Degiorgi, R. Gaal, L. Thien-Nga, R. Bacsa, J.-P. Salvetat, and L. Forró, Phys. Rev. B **61**, R2468 (2000).

[22] L. Duclaux, Carbon **40**, 1751 (2002).

[23] G. Gao, T. Çağin, and W. A. Goddard, Phys. Rev. Lett. **80**, 5556 (1998).

[24] R. S. Lee, H. J. Kim, J. E. Fischer, A. Thess, and R. E. Smalley, Nature **388**, 255 (1997).

[25] L. Grigorian, G. U. Sumanasekera, A. L. Loper, S. Fang, J. L. Allen, and P. C. Eklund, Phys. Rev. B **58**, R4195 (1998).

[26] S. Tongay, J. Hwang, D. B. Tanner, H. K. Pal, D. Maslov, and A. F. Hebard, Phys. Rev. B **81**, 115428 (2010).

[27] H. Kataura, Y. Kumazawa, Y. Maniwa, I. Umezu, S. Suzuki, Y. Ohtsuka, and Y. Achiba, Synth. Met. **103**, 2555 (1999).

[28] A. Rao, S. Bandow, E. Richter, and P. Eklund, Thin Solid Films **331**, 141 (1998).

[29] P. Ayala, R. Arenal, M. Rümmeli, A. Rubio, and T. Pichler, Carbon **48**, 575 (2010).

[30] Z. R. Ismagilov, A. E. Shalagina, O. Y. Podyacheva, A. V. Ischenko, L. S. Kibis, A. I. Boronin, Y. A. Chesalov, D. I. Kochubey, A. I. Romanenko, O. B. Anikeeva, T. I. Buryakov, and E. N. Tkachev, Carbon **47**, 1922 (2009).

[31] Samples and structural characterization details of Pyrograf III were provided by the Applied Sciences, Inc., P.O. Box 579, Cedarville, Ohio 45314.

[32] F. Wooten, *Optical Properties of Solids* (Academic Press, New York, 1972).

[33] D. B. Tanner, *Optical Effects in Solids* (Cambridge University Press, Cambridge, 2019).

[34] A. J. Gatesman, R. H. Giles, J. Waldman, L. P. Bourget, and R. S. Post, in *Diamond Optics III* (SPIE, Bellingham, WA, 1990), Vol. 1325, pp. 170–177.

[35] P. Delaney, H. J. Choi, J. Ihm, S. G. Louie, and M. L. Cohen, Nature **391**, 466 (1998).

[36] M. Ouyang, J.-L. Huang, C. L. Cheung, and C. M. Lieber, Science **292**, 702 (2001).

[37] E. F. Schubert, L. W. Tu, G. J. Zydzik, R. F. Kopf, A. Benvenuti, and M. R. Pinto, Appl. Phys. Lett. **60**, 466 (1992).

[38] G. Schuberth, F. Schäffler, M. Besson, G. Abstreiter, and E. Gornik, Appl. Phys. Lett. **59**, 3318 (1991).

[39] A. Chin, T. Y. Chang, A. Ourmazd, and E. M. Monberg, Appl. Phys. Lett. **58**, 968 (1991).

[40] J. Cowley, P. Nikolaev, A. Thess, and R. E. Smalley, Chem. Phys. Lett. **265**, 379 (1997).

[41] O. Hilt, H. B. Brom, and M. Ahlskog, Phys. Rev. B **61**, R5129 (2000).

[42] P. Petit, E. Jouguelet, J. E. Fischer, A. G. Rinzler, and R. E. Smalley, Phys. Rev. B **56**, 9275 (1997).

[43] C. A. Klein and W. D. Straub, Phys. Rev. **123**, 1581 (1961).

[44] A. Bezryadin, A. R. M. Verschueren, S. J. Tans, and C. Dekker, Phys. Rev. Lett. **80**, 4036 (1998).